Study of high-multiplicity three-prong and five-prong τ decays at *BABAR*

J. P. Lees,[1] V. Poireau,[1] V. Tisserand,[1] J. Garra Tico,[2] E. Grauges,[2] A. Palano,[3a,3b] G. Eigen,[4] B. Stugu,[4] D. N. Brown,[5] L. T. Kerth,[5] Yu. G. Kolomensky,[5] G. Lynch,[5] H. Koch,[6] T. Schroeder,[6] D. J. Asgeirsson,[7] C. Hearty,[7] T. S. Mattison,[7] J. A. McKenna,[7] R. Y. So,[7] A. Khan,[8] V. E. Blinov,[9] A. R. Buzykaev,[9] V. P. Druzhinin,[9] V. B. Golubev,[9] E. A. Kravchenko,[9] A. P. Onuchin,[9] S. I. Serednyakov,[9] Yu. I. Skovpen,[9] E. P. Solodov,[9] K. Yu. Todyshev,[9] A. N. Yushkov,[9] M. Bondioli,[10] D. Kirkby,[10] A. J. Lankford,[10] M. Mandelkern,[10] H. Atmacan,[11] J. W. Gary,[11] F. Liu,[11] O. Long,[11] G. M. Vitug,[11] C. Campagnari,[12] T. M. Hong,[12] D. Kovalskyi,[12] J. D. Richman,[12] C. A. West,[12] A. M. Eisner,[13] J. Kroseberg,[13] W. S. Lockman,[13] A. J. Martinez,[13] B. A. Schumm,[13] A. Seiden,[13] D. S. Chao,[14] C. H. Cheng,[14] B. Echenard,[14] K. T. Flood,[14] D. G. Hitlin,[14] P. Ongmongkolkul,[14] F. C. Porter,[14] A. Y. Rakitin,[14] R. Andreassen,[15] Z. Huard,[15] B. T. Meadows,[15] M. D. Sokoloff,[15] L. Sun,[15] P. C. Bloom,[16] W. T. Ford,[16] A. Gaz,[16] U. Nauenberg,[16] J. G. Smith,[16] S. R. Wagner,[16] R. Ayad,[17,*] W. H. Toki,[17] B. Spaan,[18] K. R. Schubert,[19] R. Schwierz,[19] D. Bernard,[20] M. Verderi,[20] P. J. Clark,[21] S. Playfer,[21] D. Bettoni,[22a] C. Bozzi,[22a] R. Calabrese,[22a,22b] G. Cibinetto,[22a,22b] E. Fioravanti,[22a,22b] I. Garzia,[22a,22b] E. Luppi,[22a,22b] M. Munerato,[22a,22b] L. Piemontese,[22a] V. Santoro,[22a] R. Baldini-Ferroli,[23] A. Calcaterra,[23] R. de Sangro,[23] G. Finocchiaro,[23] P. Patteri,[23] I. M. Peruzzi,[23,†] M. Piccolo,[23] M. Rama,[23] A. Zallo,[23] R. Contri,[24a,24b] E. Guido,[24a,24b] M. Lo Vetere,[24a,24b] M. R. Monge,[24a,24b] S. Passaggio,[24a] C. Patrignani,[24a,24b] E. Robutti,[24a] B. Bhuyan,[25] V. Prasad,[25] C. L. Lee,[26] M. Morii,[26] A. J. Edwards,[27] A. Adametz,[28] U. Uwer,[28] H. M. Lacker,[29] T. Lueck,[29] P. D. Dauncey,[30] U. Mallik,[31] C. Chen,[32] J. Cochran,[32] W. T. Meyer,[32] S. Prell,[32] A. E. Rubin,[32] A. V. Gritsan,[33] Z. J. Guo,[33] N. Arnaud,[34] M. Davier,[34] D. Derkach,[34] G. Grosdidier,[34] F. Le Diberder,[34] A. M. Lutz,[34] B. Malaescu,[34] P. Roudeau,[34] M. H. Schune,[34] A. Stocchi,[34] G. Wormser,[34] D. J. Lange,[35] D. M. Wright,[35] C. A. Chavez,[36] J. P. Coleman,[36] J. R. Fry,[36] E. Gabathuler,[36] D. E. Hutchcroft,[36] D. J. Payne,[36] C. Touramanis,[36] A. J. Bevan,[37] F. Di Lodovico,[37] R. Sacco,[37] M. Sigamani,[37] G. Cowan,[38] D. N. Brown,[39] C. L. Davis,[39] A. G. Denig,[40] M. Fritsch,[40] W. Gradl,[40] K. Griessinger,[40] A. Hafner,[40] E. Prencipe,[40] R. J. Barlow,[41,‡] G. Jackson,[41] G. D. Lafferty,[41] E. Behn,[42] R. Cenci,[42] B. Hamilton,[42] A. Jawahery,[42] D. A. Roberts,[42] C. Dallapiccola,[43] R. Cowan,[44] D. Dujmic,[44] G. Sciolla,[44] R. Cheaib,[45] D. Lindemann,[45] P. M. Patel,[45,§] S. H. Robertson,[45] P. Biassoni,[46a,46b] N. Neri,[46a] F. Palombo,[46a,46b] S. Stracka,[46a,46b] L. Cremaldi,[47] R. Godang,[47,‖] R. Kroeger,[47] P. Sonnek,[47] D. J. Summers,[47] X. Nguyen,[48] M. Simard,[48] P. Taras,[48] G. De Nardo,[49a,49b] D. Monorchio,[49a,49b] G. Onorato,[49a,49b] C. Sciacca,[49a,49b] M. Martinelli,[50] G. Raven,[50] C. P. Jessop,[51] J. M. LoSecco,[51] W. F. Wang,[51] K. Honscheid,[52] R. Kass,[52] J. Brau,[53] R. Frey,[53] N. B. Sinev,[53] D. Strom,[53] E. Torrence,[53] E. Feltresi,[54a,54b] N. Gagliardi,[54a,54b] M. Margoni,[54a,54b] M. Morandin,[54a] M. Posocco,[54a] M. Rotondo,[54a] G. Simi,[54a] F. Simonetto,[54a,54b] R. Stroili,[54a,54b] S. Akar,[55] E. Ben-Haim,[55] M. Bomben,[55] G. R. Bonneaud,[55] H. Briand,[55] G. Calderini,[55] J. Chauveau,[55] O. Hamon,[55] Ph. Leruste,[55] G. Marchiori,[55] J. Ocariz,[55] S. Sitt,[55] M. Biasini,[56a,56b] E. Manoni,[56a,56b] S. Pacetti,[56a,56b] A. Rossi,[56a,56b] C. Angelini,[57a,57b] G. Batignani,[57a,57b] S. Bettarini,[57a,57b,¶] M. Carpinelli,[57a,57b,¶] G. Casarosa,[57a,57b] A. Cervelli,[57a,57b] F. Forti,[57a,57b] M. A. Giorgi,[57a,57b] A. Lusiani,[57a,57c] B. Oberhof,[57a,57b] E. Paoloni,[57a,57b] A. Perez,[57a] G. Rizzo,[57a,57b] J. J. Walsh,[57a] D. Lopes Pegna,[58] J. Olsen,[58] A. J. S. Smith,[58] A. V. Telnov,[58] F. Anulli,[59a] R. Faccini,[59a,59b] F. Ferrarotto,[59a] F. Ferroni,[59a,59b] M. Gaspero,[59a,59b] L. Li Gioi,[59a] M. A. Mazzoni,[59a] G. Piredda,[59a] C. Bünger,[60] O. Grünberg,[60] T. Hartmann,[60] T. Leddig,[60] H. Schröder,[60,§] C. Voss,[60] R. Waldi,[60] T. Adye,[61] E. O. Olaiya,[61] F. F. Wilson,[61] S. Emery,[62] G. Hamel de Monchenault,[62] G. Vasseur,[62] Ch. Yèche,[62] D. Aston,[63] D. J. Bard,[63] R. Bartoldus,[63] J. F. Benitez,[63] C. Cartaro,[63] M. R. Convery,[63] J. Dorfan,[63] G. P. Dubois-Felsmann,[63] W. Dunwoodie,[63] M. Ebert,[63] R. C. Field,[63] M. Franco Sevilla,[63] B. G. Fulsom,[63] A. M. Gabareen,[63] M. T. Graham,[63] P. Grenier,[63] C. Hast,[63] W. R. Innes,[63] M. H. Kelsey,[63] P. Kim,[63] M. L. Kocian,[63] D. W. G. S. Leith,[63] P. Lewis,[63] B. Lindquist,[63] S. Luitz,[63] V. Luth,[63] H. L. Lynch,[63] D. B. MacFarlane,[63] D. R. Muller,[63] H. Neal,[63] S. Nelson,[63] M. Perl,[63] T. Pulliam,[63] B. N. Ratcliff,[63] A. Roodman,[63] A. A. Salnikov,[63] R. H. Schindler,[63] A. Snyder,[63] D. Su,[63] M. K. Sullivan,[63] J. Va'vra,[63] A. P. Wagner,[63] W. J. Wisniewski,[63] M. Wittgen,[63] D. H. Wright,[63] H. W. Wulsin,[63] C. C. Young,[63] V. Ziegler,[63] W. Park,[64] M. V. Purohit,[64] R. M. White,[64] J. R. Wilson,[64] A. Randle-Conde,[65] S. J. Sekula,[65] M. Bellis,[66] P. R. Burchat,[66] T. S. Miyashita,[66] M. S. Alam,[67] J. A. Ernst,[67] R. Gorodeisky,[68] N. Guttman,[68] D. R. Peimer,[68] A. Soffer,[68] P. Lund,[69] S. M. Spanier,[69] J. L. Ritchie,[70] A. M. Ruland,[70] R. F. Schwitters,[70] B. C. Wray,[70] J. M. Izen,[71] X. C. Lou,[71] F. Bianchi,[72a,72b] D. Gamba,[72a,72b] S. Zambito,[72a,72b] L. Lanceri,[73a,73b] L. Vitale,[73a,73b] F. Martinez-Vidal,[74] A. Oyanguren,[74] H. Ahmed,[75] J. Albert,[75] Sw. Banerjee,[75] F. U. Bernlochner,[75] H. H. F. Choi,[75] G. J. King,[75] R. Kowalewski,[75] M. J. Lewczuk,[75] I. M. Nugent,[75] J. M. Roney,[75] R. J. Sobie,[75] N. Tasneem,[75] T. J. Gershon,[76] P. F. Harrison,[76] T. E. Latham,[76] E. M. T. Puccio,[76] H. R. Band,[77] S. Dasu,[77] Y. Pan,[77] R. Prepost,[77] and S. L. Wu[77]

(*BABAR* Collaboration)

[1]*Laboratoire d'Annecy-le-Vieux de Physique des Particules (LAPP), Université de Savoie, CNRS/IN2P3, F-74941 Annecy-Le-Vieux, France*
[2]*Facultat de Fisica, Departament ECM, Universitat de Barcelona, E-08028 Barcelona, Spain*
[3a]*INFN Sezione di Bari, I-70126 Bari, Italy*
[3b]*Dipartimento di Fisica, Università di Bari, I-70126 Bari, Italy*
[4]*Institute of Physics, University of Bergen, N-5007 Bergen, Norway*
[5]*Lawrence Berkeley National Laboratory and University of California, Berkeley, California 94720, USA*
[6]*Institut für Experimentalphysik 1, Ruhr Universität Bochum, D-44780 Bochum, Germany*
[7]*University of British Columbia, Vancouver, British Columbia V6T 1Z1, Canada*
[8]*Brunel University, Uxbridge, Middlesex UB8 3PH, United Kingdom*
[9]*Budker Institute of Nuclear Physics, Novosibirsk 630090, Russia*
[10]*University of California at Irvine, Irvine, California 92697, USA*
[11]*University of California at Riverside, Riverside, California 92521, USA*
[12]*University of California at Santa Barbara, Santa Barbara, California 93106, USA*
[13]*Institute for Particle Physics, University of California at Santa Cruz, Santa Cruz, California 95064, USA*
[14]*California Institute of Technology, Pasadena, California 91125, USA*
[15]*University of Cincinnati, Cincinnati, Ohio 45221, USA*
[16]*University of Colorado, Boulder, Colorado 80309, USA*
[17]*Colorado State University, Fort Collins, Colorado 80523, USA*
[18]*Fakultät Physik, Technische Universität Dortmund, D-44221 Dortmund, Germany*
[19]*Institut für Kern- und Teilchenphysik, Technische Universität Dresden, D-01062 Dresden, Germany*
[20]*Laboratoire Leprince-Ringuet, Ecole Polytechnique, CNRS/IN2P3, F-91128 Palaiseau, France*
[21]*University of Edinburgh, Edinburgh EH9 3JZ, United Kingdom*
[22a]*INFN Sezione di Ferrara, I-44100 Ferrara, Italy*
[22b]*Dipartimento di Fisica, Università di Ferrara, I-44100 Ferrara, Italy*
[23]*INFN Laboratori Nazionali di Frascati, I-00044 Frascati, Italy*
[24a]*INFN Sezione di Genova, I-16146 Genova, Italy*
[24b]*Dipartimento di Fisica, Università di Genova, I-16146 Genova, Italy*
[25]*Indian Institute of Technology Guwahati, Guwahati, Assam 781 039, India*
[26]*Harvard University, Cambridge, Massachusetts 02138, USA*
[27]*Harvey Mudd College, Claremont, California 91711, USA*
[28]*Universität Heidelberg, Physikalisches Institut, Philosophenweg 12, D-69120 Heidelberg, Germany*
[29]*Institut für Physik, Humboldt-Universität zu Berlin, Netwonstrausse 15, D-12489 Berlin, Germany*
[30]*Imperial College London, London SW7 2AZ, United Kingdom*
[31]*University of Iowa, Iowa City, Iowa 52242, USA*
[32]*Iowa State University, Ames, Iowa 50011-3160, USA*
[33]*Johns Hopkins University, Baltimore, Maryland 21218, USA*
[34]*Laboratoire de l'Accélérateur Linéaire, IN2P3/CNRS et Université Paris-Sud 11, Centre Scientifique d'Orsay, B. P. 34, F-91898 Orsay Cedex, France*
[35]*Lawrence Livermore National Laboratory, Livermore, California 94550, USA*
[36]*University of Liverpool, Liverpool L69 7ZE, United Kingdom*
[37]*Queen Mary, University of London, London E1 4NS, United Kingdom*
[38]*Royal Holloway and Bedford New College, University of London, Egham, Surrey TW20 0EX, United Kingdom*
[39]*University of Louisville, Louisville, Kentucky 40292, USA*
[40]*Institut für Kernphysik, Johannes Gutenberg-Universität Mainz, D-55099 Mainz, Germany*
[41]*University of Manchester, Manchester M13 9PL, United Kingdom*
[42]*University of Maryland, College Park, Maryland 20742, USA*
[43]*University of Massachusetts, Amherst, Massachusetts 01003, USA*
[44]*Massachusetts Institute of Technology, Laboratory for Nuclear Science, Cambridge, Massachusetts 02139, USA*
[45]*McGill University, Montréal, Québec H3A 2T8, Canada*
[46a]*INFN Sezione di Milano, I-20133 Milano, Italy*
[46b]*Dipartimento di Fisica, Università di Milano, I-20133 Milano, Italy*
[47]*University of Mississippi, University, Mississippi 38677, USA*
[48]*Université de Montréal, Physique des Particules, Montréal, Québec H3C 3J7, Canada*
[49a]*INFN Sezione di Napoli, I-80126 Napoli, Italy*

[49b]Dipartimento di Scienze Fisiche, Università di Napoli Federico II, I-80126 Napoli, Italy
[50]NIKHEF, National Institute for Nuclear Physics and High Energy Physics, NL-1009 DB Amsterdam, The Netherlands
[51]University of Notre Dame, Notre Dame, Indiana 46556, USA
[52]Ohio State University, Columbus, Ohio 43210, USA
[53]University of Oregon, Eugene, Oregon 97403, USA
[54a]INFN Sezione di Padova, I-35131 Padova, Italy
[54b]Dipartimento di Fisica, Università di Padova, I-35131 Padova, Italy
[55]Laboratoire de Physique Nucléaire et de Hautes Energies, IN2P3/CNRS, Université Pierre et Marie Curie-Paris6, Université Denis Diderot-Paris7, F-75252 Paris, France
[56a]INFN Sezione di Perugia, I-06100 Perugia, Italy
[56b]Dipartimento di Fisica, Università di Perugia, I-06100 Perugia, Italy
[57a]INFN Sezione di Pisa, I-06100 Perugia, Italy
[57b]Dipartimento di Fisica, Università di Pisa, I-06100 Perugia, Italy
[57c]Scuola Normale Superiore di Pisa, I-56127 Pisa, Italy
[58]Princeton University, Princeton, New Jersey 08544, USA
[59a]INFN Sezione di Roma, I-00185 Roma, Italy
[59b]Dipartimento di Fisica, Università di Roma La Sapienza, I-00185 Roma, Italy
[60]Universität Rostock, D-18051 Rostock, Germany
[61]Rutherford Appleton Laboratory, Chilton, Didcot, Oxon OX11 0QX, United Kingdom
[62]CEA, Irfu, SPP, Centre de Saclay, F-91191 Gif-sur-Yvette, France
[63]SLAC National Accelerator Laboratory, Stanford, California 94309, USA
[64]University of South Carolina, Columbia, South Carolina 29208, USA
[65]Southern Methodist University, Dallas, Texas 75275, USA
[66]Stanford University, Stanford, California 94305-4060, USA
[67]State University of New York, Albany, New York 12222, USA
[68]Tel Aviv University, School of Physics and Astronomy, Tel Aviv 69978, Israel
[69]University of Tennessee, Knoxville, Tennessee 37996, USA
[70]University of Texas at Austin, Austin, Texas 78712, USA
[71]University of Texas at Dallas, Richardson, Texas 75083, USA
[72a]INFN Sezione di Torino, I-10125 Torino, Italy
[72b]Dipartimento di Fisica Sperimentale, Università di Torino, I-10125 Torino, Italy
[73a]INFN Sezione di Trieste, I-34127 Trieste, Italy
[73b]Dipartimento di Fisica, Università di Trieste, I-34127 Trieste, Italy
[74]IFIC, Universitat de Valencia-CSIC, E-46071 Valencia, Spain
[75]University of Victoria, Victoria, British Columbia V8W 3P6, Canada
[76]Department of Physics, University of Warwick, Coventry CV4 7AL, United Kingdom
[77]University of Wisconsin, Madison, Wisconsin 53706, USA

(Received 14 September 2012; published 27 November 2012)

We present measurements of the branching fractions of three-prong and five-prong τ decay modes using a sample of 430 million τ lepton pairs, corresponding to an integrated luminosity of 468 fb^{-1}, collected with the *BABAR* detector at the PEP-II asymmetric-energy e^+e^- storage rings at SLAC National Accelerator Laboratory. The $\tau^- \to (3\pi)^-\eta\nu_\tau$, $\tau^- \to (3\pi)^-\omega\nu_\tau$, and $\tau^- \to \pi^- f_1(1285)\nu_\tau$ branching fractions are presented, as well as a new limit on the branching fraction of the second-class current decay $\tau^- \to \pi^-\eta'(958)\nu_\tau$. We search for the decay mode $\tau^- \to K^-\eta'(958)\nu_\tau$ and for five-prong decay modes with kaons, and place the first upper limits on their branching fractions.

DOI: 10.1103/PhysRevD.86.092010 PACS numbers: 13.35.Dx, 14.60.Fg

I. INTRODUCTION

Study of the three-prong and five-prong decay modes of the τ lepton, where "prong" refers to the number of charged hadrons (π or K) in the final state, allows one to test the Standard Model and search for evidence of new physics. The large τ lepton data sample collected by the *BABAR* experiment provides an opportunity to perform a comprehensive study of rare, high multiplicity decay modes and to search for forbidden processes.

[*]Now at the University of Tabuk, Tabuk 71491, Saudi Arabia.
[†]Also with Università di Perugia, Dipartimento di Fisica, Perugia, Italy.
[‡]Now at the University of Huddersfield, Huddersfield HD1 3DH, UK.
[§]Deceased.
[‖]Now at University of South Alabama, Mobile, Alabama 36688, USA.
[¶]Also with Università di Sassari, Sassari, Italy.

We present measurements of the $\tau^- \to (3\pi)^- \eta \nu_\tau$, $\tau^- \to (3\pi)^- \omega \nu_\tau$, and $\tau^- \to \pi^- f_1 \nu_\tau$ branching fractions. We use the primary decay modes of the η, $\omega(782)$, and $f_1(1258)$ mesons: $\eta \to \gamma\gamma$, $\eta \to \pi^+\pi^-\pi^0$, $\eta \to 3\pi^0$, $\omega \to \pi^-\pi^+\pi^0$, $f_1 \to 2\pi^+2\pi^-$, and $f_1 \to \pi^+\pi^-\eta$. No other narrow resonances are observed. We measure the branching fractions of the nonresonant decays, where the nonresonant category includes possible contributions from broad resonances. We present a new limit on the branching fractions of the second-class current decay $\tau^- \to \pi^- \eta'(958)\nu_\tau$, and the first limits on the allowed first-class current decays $\tau^- \to K^- \eta'(958)\nu_\tau$ and $\tau^- \to \pi^-\pi^0\eta'(958)\nu_\tau$. Finally, we present the first limits on the branching fractions of five-prong decay modes in which one or more of the charged hadrons is a charged kaon. Note that the branching fractions exclude the contribution of $K^0_S \to \pi^+\pi^-$ decays. Throughout this paper, charge conjugation is implied.

This analysis is based on data recorded with the *BABAR* detector at the PEP-II asymmetric-energy e^+e^- storage rings operated at the SLAC National Accelerator Laboratory. With an integrated luminosity ($\mathcal{L}$) of 424 and 44 fb^{-1} recorded at center-of-mass (CM) energies of 10.58 and 10.54 GeV, respectively, and an $e^+e^- \to \tau^+\tau^-$ cross section of $\sigma_{\tau^+\tau^-} = (0.919 \pm 0.003)$ nb [1], the data sample contains 430 million τ pairs.

The *BABAR* detector is described in detail in Ref. [2]. Charged-particle momenta are measured with a five-layer double-sided silicon vertex tracker and a 40-layer drift chamber, both operating in the 1.5 T magnetic field of a superconducting solenoid. Information from a detector of internally reflected Cerenkov light is used in conjunction with specific energy loss measurements from the tracking detectors to identify charged pions and kaons [3]. Photons are reconstructed from energy clusters deposited in a CsI (TI) electromagnetic calorimeter. Electrons are identified by combining tracking and calorimeter information. An instrumented magnetic flux return is used to identify muons.

The background contamination and selection efficiencies are determined using Monte Carlo simulation. The τ-pair production is simulated with the KK2F event generator [4]. The τ decays, continuum $q\bar{q}$ events ($q = udsc$), and final-state radiative effects are modeled with the Tauola [5], JETSET [6], and Photos [7] generators, respectively. Dedicated samples of $\tau^+\tau^-$ events are created using the Tauola or EVTGEN [8] programs, with one of the τ leptons allowed to decay to any mode while the other τ decays to a specific final state. The detector response is simulated with GEANT4 [9]. All Monte Carlo events are processed through a full simulation of the *BABAR* detector and are reconstructed in the same manner as the data.

II. EVENT SELECTION

The τ pair is produced back-to-back in the e^+e^- CM frame. The decay products of the two τ leptons can thus be separated from each other by dividing the event into two hemispheres: the "signal" hemisphere and the "tag" hemisphere. The separation is performed using the event thrust axis [10], which is calculated using all charged particle and photon candidates in the event.

We select events where one hemisphere (tag) contains exactly one track while the other hemisphere (signal) contains exactly three or five tracks with total charge opposite to that of the tag hemisphere. The event is rejected if any pair of oppositely charged tracks is consistent with a photon conversion. The component of the momentum transverse to the beam axis for each of the tracks must be greater than 0.1 GeV/c in the laboratory frame. All tracks are required to have a point of closest approach to the interaction region less than 1.5 cm in the plane transverse to the beam axis and less than 2.5 cm in the direction along that axis. This requirement eliminates K^0_S mesons that decay to $\pi^+\pi^-$ at points distant from the e^+e^- collision point.

To reduce backgrounds from non-τ pair events, we require that the momentum of the charged particle in the tag hemisphere be less than 4 GeV/c in the CM frame and that the charged particle be identified as an electron or a muon. The $q\bar{q}$ background is suppressed by requiring that there be at most one energetic ($E > 1$ GeV) electromagnetic calorimeter cluster in the tag hemisphere that is not associated with a track. Additional background suppression is achieved by requiring the magnitude of the event thrust to lie between 0.92 and 0.99.

Neutral pion and eta candidates are reconstructed from two photon candidates, each with energy greater than 30 MeV in the laboratory frame; the invariant mass of the π^0 (η) is required to be between 0.115 (0.35) and 0.150 (0.70) GeV/c^2. Neutral pion candidates are reconstructed in the signal hemisphere. If a photon candidate meets the invariant mass requirement with multiple photon candidates, then the neutral pion candidate with invariant mass closest to the nominal π^0 mass [11] is selected. The search for additional pion candidates is repeated using the remaining photon candidates. The residual photon clusters in the signal hemisphere are used to search for $\eta \to \gamma\gamma$ candidates. In the case of multiple η candidates, the candidate with invariant mass closest to the nominal η mass is selected. We reject events in which the invariant mass M formed from the system of charged particles, π^0, and η candidates, all in the signal hemisphere, exceeds 1.8 GeV/c^2.

The branching fractions are calculated using the expression $\mathcal{B} = N_X/(2N\varepsilon)$ where N_X is the number of candidates after background subtraction, N is the number of τ pairs produced, and ε is the selection efficiency. N is determined from the product of the integrated luminosity and the $e^+e^- \to \tau^+\tau^-$ cross section. The uncertainty of N is estimated to be 1%. The selection efficiencies are determined from the signal Monte Carlo samples. The

uncertainty on the selection efficiencies includes 0.5% per track on the track reconstruction efficiency, as well as particle identification (PID) selection uncertainties. From studies conducted on real and simulated events, the uncertainties on the charged particle identification selectors are estimated to be 1% for electrons, 2.5% for muons, 0.5% for pions, and 1.8% for kaons. The combined electron and muon particle identification uncertainty is estimated to be 1.6% based on the composition of the event samples. The uncertainty on the $\pi^0 \to \gamma\gamma$ and $\eta \to \gamma\gamma$ reconstruction efficiency is estimated to be 3% per candidate.

III. RESULTS

We present measurements of τ decays to a system with η, f_1 and ω resonances in Secs. III A, III B, and III C, respectively. Decays with these resonances do not account for all three-prong or five-prong τ decay modes, as discussed below, and we present measurements of the τ branching fractions through nonresonant modes in Sec. III D. Section III E presents a search for τ decays with an η' (958) meson, while Sec. III F presents a search for decays with either one or two charged kaons.

A. $\tau^- \to (3\pi)^- \eta\nu_\tau$

The $\tau^- \to 2\pi^-\pi^+\eta\nu_\tau$ mode is studied in the $\eta \to \gamma\gamma$, $\eta \to \pi^+\pi^-\pi^0$, and $\eta \to 3\pi^0$ final states, while the $\tau^- \to \pi^- 2\pi^0\eta\nu_\tau$ mode is studied in the $\eta \to \pi^+\pi^-\pi^0$ final state.

The event yields are determined by fitting the η mass peak in the $\gamma\gamma$, $\pi^+\pi^-\pi^0$, and $3\pi^0$ invariant mass distributions (see Fig. 1). The fit uses a Novosibirsk function [12] (a Gaussian distribution with a tail parameter) for the η and a polynomial function for the background.

The Monte Carlo simulation indicates that some of the entries in the η peak are from $e^+e^- \to q\bar{q}$ events. Control samples, obtained by reversing the requirement on the invariant mass of the observed decay products ($M > 1.8\ \mathrm{GeV}/c^2$), are used to validate the background estimate. The expected background is corrected by the ratio of data to Monte Carlo events, and the statistical uncertainty of the ratio is included in the background systematic uncertainty. This method of validating the $q\bar{q}$ background estimate is used for all decays and is not mentioned in the later sections.

The reconstruction efficiencies are determined from fits to the signal Monte Carlo samples. The $\tau^- \to \pi^- 2\pi^0\eta\nu_\tau$ sample is generated using a phase-space model for the final-state particles. The $\tau^- \to 2\pi^-\pi^+\eta\nu_\tau$ sample is composed of $\tau^- \to \pi^- f_1\nu_\tau$ ($f_1 \to \pi^+\pi^-\eta$) decays and decays without an intermediate resonance. The $\tau^- \to 2\pi^-\pi^+\eta\nu_\tau$ (excluding f_1) and $\tau^- \to \pi^- f_1\nu_\tau$ efficiencies are the same for $\eta \to \pi^+\pi^-\pi^0$ and $\eta \to 3\pi^0$ events, whereas a slight difference is observed for $\eta \to \gamma\gamma$ events and a 2.5% uncertainty is added to the selection efficiency systematic for this mode. In addition, a 4% uncertainty is added to the $\tau^- \to 2\pi^-\pi^+\eta\nu_\tau$ selection efficiency for the $\eta \to \pi^+\pi^-\pi^0$ mode to take into account variations observed for different fits.

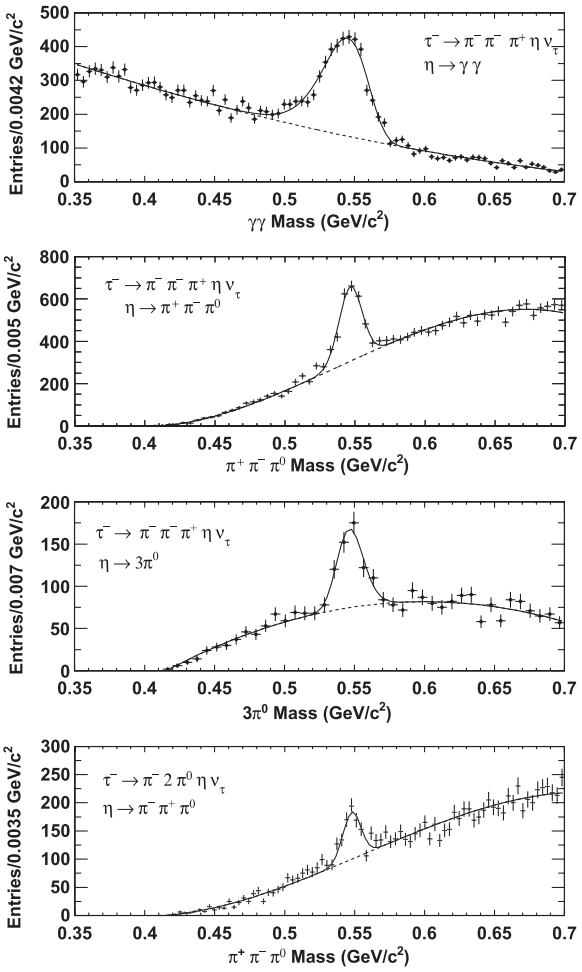

FIG. 1. The $\gamma\gamma$, $\pi^+\pi^-\pi^0$, and $3\pi^0$ invariant mass distributions for $\tau^- \to 2\pi^-\pi^+\eta\nu_\tau$ decay candidates, and the $\pi^+\pi^-\pi^0$ invariant mass distribution for $\tau^- \to \pi^- 2\pi^0\eta\nu_\tau$ decay candidates, after all selection criteria are applied. The solid lines represent the fit to the η peak and background. The dashed lines show the extrapolation of the background function under the η peak.

The three determinations of the $\tau^- \to 2\pi^-\pi^+\eta\nu_\tau$ branching fraction are found to be in good agreement (see Table I) and we therefore calculate a weighted average. The statistical and systematic uncertainties on the average are obtained by combining the individual uncertainties in quadrature, accounting for correlations between the systematic terms. The weighted average (inclusive of $\tau^- \to \pi^- f_1\nu_\tau$) is found to be

$$\mathcal{B}(\tau^- \to 2\pi^-\pi^+\eta\nu_\tau) = (2.25 \pm 0.07 \pm 0.12) \times 10^{-4}.$$

Hereinafter, when two uncertainties are quoted, the first is statistical and the second is systematic. The average

TABLE I. Results and branching fractions for $\tau^- \to (3\pi)^- \eta \nu_\tau$ decays.

Decay mode	$\tau^- \to 2\pi^-\pi^+\eta\nu_\tau$ $\eta \to \gamma\gamma$	$\tau^- \to 2\pi^-\pi^+\eta\nu_\tau$ $\eta \to \pi^+\pi^-\pi^0$	$\tau^- \to 2\pi^-\pi^+\eta\nu_\tau$ $\eta \to 3\pi^0$	$\tau^- \to \pi^- 2\pi^0\eta\nu_\tau$ $\eta \to \pi^+\pi^-\pi^0$
Branching fraction (10^{-4})	$2.10 \pm 0.09 \pm 0.13$	$2.37 \pm 0.12 \pm 0.18$	$2.54 \pm 0.27 \pm 0.25$	$2.01 \pm 0.34 \pm 0.22$
Data events	2887 ± 103	1440 ± 68	315 ± 34	381 ± 45
χ^2/NDF	107/76	60/52	31/34	95/75
Selection efficiency	$(3.83 \pm 0.11)\%$	$(2.97 \pm 0.12)\%$	$(0.42 \pm 0.01)\%$	$(0.75 \pm 0.02)\%$
Background events	131 ± 29	65 ± 38	13 ± 7	83 ± 12
Systematic uncertainties (%)				
Tracking efficiency	2.7	3.8	2.7	2.7
π^0 and η PID	3.0	3.0	9.0	9.0
Pion PID	1.5	2.5	1.5	1.5
Lepton-tag PID	1.6	1.6	1.6	1.6
N	1.0	1.0	1.0	1.0
Selection efficiency	3.9	4.0	2.8	2.7
Background	1.0	2.8	2.3	4.0
$\mathcal{B}(\eta \to \gamma\gamma)$	1.0	...	...	...
$\mathcal{B}(\eta \to \pi^+\pi^-\pi^0)$	...	1.8	...	1.8
$\mathcal{B}(\eta \to 3\pi^0)$	...	...	0.9	...
Total (%)	6.3	7.4	10	11

branching fraction (exclusive of $\tau^- \to \pi^- f_1 \nu_\tau$) is determined to be $(0.99 \pm 0.09 \pm 0.13) \times 10^{-4}$ and is obtained using the branching fraction (inclusive of $\tau^- \to \pi^- f_1 \nu_\tau$), given above, and subtracting the product branching fraction $\mathcal{B}(\tau^- \to \pi^- f_1 \nu_\tau) \times \mathcal{B}(f_1 \to \pi^+\pi^-\eta)$ presented in the next section.

The $\tau^- \to \pi^- 2\pi^0 \eta \nu_\tau$ branching fraction is found to be

$$\mathcal{B}(\tau^- \to \pi^- 2\pi^0 \eta \nu_\tau) = (2.01 \pm 0.34 \pm 0.22) \times 10^{-4}.$$

Naively, the ratio of the $\tau^- \to 2\pi^-\pi^+\eta\nu_\tau$ to $\tau^- \to \pi^- 2\pi^0\eta\nu_\tau$ branching fractions is expected to be two if the decay is dominated by the $\tau^- \to \pi^- f_1 \nu_\tau$ decay mode (based on the f_1 branching fractions [11]). The data do not support this expectation.

Our previous measurement of the $\tau^- \to 2\pi^-\pi^+\eta\nu_\tau$ branching fraction $(1.60 \pm 0.05 \pm 0.11) \times 10^{-4}$ [13], which is based on the $\eta \to \gamma\gamma$ mode only, is superseded by this measurement. The fit used in the previous analysis was performed using a narrower range in the invariant mass distribution (0.47–0.63 GeV/c^2) defined in a predetermined η selector. The narrow fit range resulted in an incorrect description of the background distribution giving the wrong number of η candidates. The current work uses wider fit range (0.30–0.70 GeV/c^2) and the background distribution is well described.

The $\tau^- \to 2\pi^-\pi^+\eta\nu_\tau$ and $\tau^- \to \pi^- 2\pi^0\eta\nu_\tau$ branching fractions are in good agreement with the results from the CLEO collaboration, $(2.3 \pm 0.5) \times 10^{-4}$ and $(1.5 \pm 0.5) \times 10^{-4}$, respectively [14]. Li predicts a larger $\tau^- \to 2\pi^-\pi^+\eta\nu_\tau$ branching fraction, 2.93×10^{-4} [15].

B. $\tau^- \to \pi^- f_1 \nu_\tau$

The branching fraction of $\tau^- \to \pi^- f_1 \nu_\tau$ and the mass of the f_1 meson are measured using the $f_1 \to 2\pi^+2\pi^-$ and $f_1 \to \pi^+\pi^-\eta$ decay modes, where the $f_1 \to \pi^+\pi^-\eta$ decay is reconstructed using $\eta \to \gamma\gamma$, $\eta \to \pi^+\pi^-\pi^0$, and $\eta \to 3\pi^0$ events. The criteria used to select the $\tau^- \to \pi^- f_1 \nu_\tau$ decays for the branching fraction measurement are described earlier. We modify the selection for the mass measurement, dropping the requirement that the track in the tag hemisphere be a lepton and the restriction on the number of photon candidates in the tag hemisphere, to increase the size of the event sample.

The numbers of $\tau^- \to \pi^- f_1 \nu_\tau$ candidates are determined by fitting the f_1 peak in the $2\pi^+2\pi^-$ and $\pi^+\pi^-\eta$ invariant mass distributions (see Fig. 2). The f_1 line shape is expected to be a Breit-Wigner distribution, modified by the limited phase space. Previous studies show that the $f_1 \to a_0^- \pi^+$ ($a_0^-(980) \to \pi^-\eta$) channel appears to account for all $f_1 \to \pi^+\pi^-\eta$ decays [16]. The mass of the $\pi a_0(980)$ system and the τ mass provide a lower and upper limit, respectively, on the f_1 line shape. We use the four vectors of the charged pion and $a_0(980)$ from the EVTGEN generator to determine the simulated f_1 line shape and find it to be a close approximation to the Breit-Wigner expectation. The f_1 peak is fit using this line shape convolved with a Gaussian distribution to take into account the effects of the detector resolution. The results of the fits are presented in Table II. There is no evidence for peaking background from $q\bar{q}$ events or other τ decays.

The product of the $\tau^- \to \pi^- f_1 \nu_\tau$ and $f_1 \to 2\pi^+2\pi^-$ branching fractions, and the product of the $\tau^- \to \pi^- f_1 \nu_\tau$

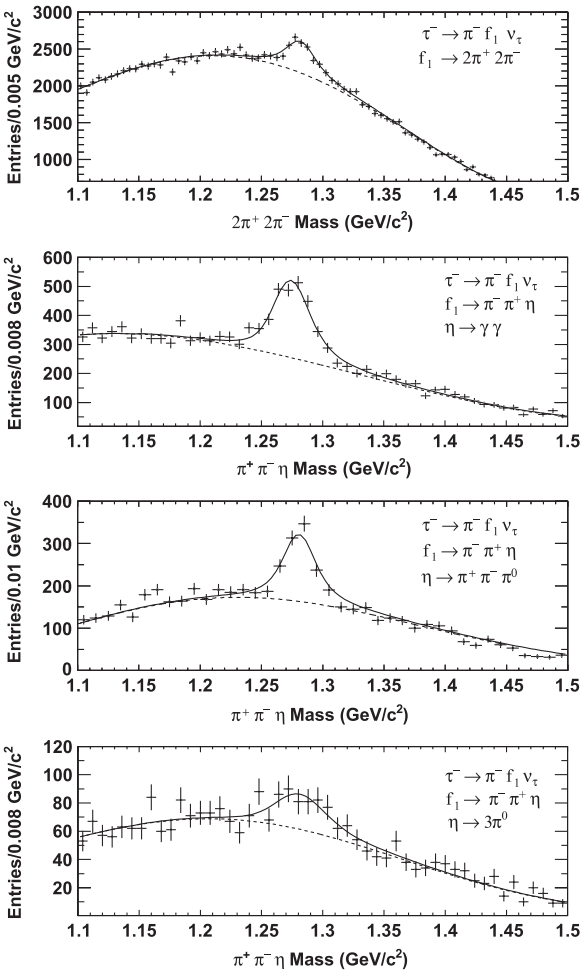

FIG. 2. The $2\pi^+2\pi^-$ and $\pi^+\pi^-\eta$ invariant mass distributions for $\tau^- \to 2\pi^-\pi^+\eta\nu_\tau$ decay candidates after all selection criteria are applied. The lower three plots are for the $\eta \to \gamma\gamma$, $\eta \to \pi^+\pi^-\pi^0$, and $\eta \to 3\pi^0$ decays. The solid lines represent the fit to the $f_1(1285)$ peak and background. The dashed lines show the extrapolation of the background function under the f_1 peak.

and $f_1 \to \pi^+\pi^-\eta$ branching fractions, are measured to be

$$\mathcal{B}(\tau^- \to \pi^- f_1 \nu_\tau)\mathcal{B}(f_1 \to 2\pi^+2\pi^-) = (5.20 \pm 0.31 \pm 0.37) \times 10^{-5},$$
$$\mathcal{B}(\tau^- \to \pi^- f_1 \nu_\tau)\mathcal{B}(f_1 \to \pi^+\pi^-\eta) = (1.26 \pm 0.06 \pm 0.06) \times 10^{-4},$$

respectively, where the second result is the weighted average of the three η modes. The $\mathcal{B}(\tau^- \to \pi^- f_1 \nu_\tau)$ branching fraction is determined to be $(4.73 \pm 0.28 \pm 0.45) \times 10^{-4}$ and $(3.60 \pm 0.18 \pm 0.23) \times 10^{-4}$, as obtained by dividing the product branching fractions by $\mathcal{B}(f_1 \to 2\pi^+2\pi^-) = 0.110^{+0.007}_{-0.006}$ and $\mathcal{B}(f_1 \to \pi^+\pi^-\eta) = 0.349^{+0.013}_{-0.015}$ [17], respectively.

Our two measured values for the $\tau^- \to \pi^- f_1 \nu_\tau$ branching fraction are consistent with each other to within two standard deviations of the combined statistical and systematic uncertainties. The ratio of the product branching fractions is used to determine the ratio of the $f_1 \to 2\pi^+2\pi^-$ and $f_1 \to \pi^+\pi^-\eta$ branching fractions as

$$\frac{\mathcal{B}(f_1 \to 2\pi^+2\pi^-)}{\mathcal{B}(f_1 \to \pi\pi\eta)} = 0.28 \pm 0.02 \pm 0.02,$$

where $\mathcal{B}(f_1 \to \pi\pi\eta) = 1.5 \times \mathcal{B}(f_1 \to \pi^+\pi^-\eta)$ based on isospin symmetry. This agrees with average value of 0.41 ± 0.14 quoted by the Particle Data Group [11] but disagrees with their fit value of 0.63 ± 0.06 [11].

The systematic uncertainties of the branching fractions are listed in Table II. We observe that the number of events in the f_1 peak in the $f_1 \to 2\pi^+2\pi^-$ sample varies by 5% for different background shapes. This variation is included as a systematic uncertainty. We also observe that the selection efficiency obtained from the Monte Carlo simulation exhibits a slight dependence on whether the f_1 decays via the $f_1 \to a_0^-\pi^+$ or the $f_1 \to \pi^+\pi^-\eta$ mode, and the variation is included as a systematic uncertainty (listed under "fit model" in Table II).

The $\tau^- \to \pi^- f_1 \nu_\tau$ branching fraction using the $f_1 \to 2\pi^+2\pi^-$ mode is consistent with the previous *BABAR* measurement (the new result supersedes the previous measurement), which is also based on the $f_1 \to 2\pi^+2\pi^-$ mode [18]. CLEO published a branching fraction of $(5.8^{+1.4}_{-1.3} \pm 1.8) \times 10^{-4}$ [19] and Li predicts a branching fraction of 2.9×10^{-4} [20].

The f_1 mass is determined by fitting the peak with a nonrelativistic Breit-Wigner function, which was used in previous measurements of the f_1 mass [11]. As a cross check, we use the energy-momentum four vectors from the generator Monte Carlo simulation, and we find the fitted mass value to be consistent with the input mass value.

We fit the invariant mass distribution in the fully reconstructed Monte Carlo samples to determine whether the result of the fit differs from the input mass of the Monte Carlo generator. The difference is used to correct the value of the invariant mass of each channel obtained from the fit and the uncertainty in the difference is included as a systematic error.

Table III and Fig. 3 show the results of the fits to the data. The last column of the table presents the mass after the application of the reconstruction correction factor. The average of these results is $M_{f_1} = (1.28025 \pm 0.00039)$ GeV/c^2, where the error is statistical.

Previous *BABAR* analyses have measured the invariant mass of resonances to be approximately 1 MeV/c^2 less than the values quoted by the Particle Data Group [11]. This shift is observed in the measurement of the mass of the f_1 meson [21] and the τ lepton [22]. The shift is attributed to the absolute energy and momentum calibration of the detector. We measure the calibration correction

TABLE II. Results and branching fractions for $\tau^- \to \pi^- f_1 \nu_\tau$ decays.

Decay mode	$f_1 \to 2\pi^+ 2\pi^-$	$f_1 \to \pi^+\pi^-\eta$ $\eta \to \gamma\gamma$	$f_1 \to \pi^+\pi^-\eta$ $\eta \to \pi^+\pi^-\pi^0$	$f_1 \to \pi^+\pi^-\eta$ $\eta \to 3\pi^0$
Branching fractions (10^{-4})				
$\mathcal{B}(\tau^- \to \pi^- f_1 \nu_\tau)\mathcal{B}(f_1 \to 2\pi^+ 2\pi^-)$	$0.520 \pm 0.031 \pm 0.037$			
$\mathcal{B}(\tau^- \to \pi^- f_1 \nu_\tau)\mathcal{B}(f_1 \to \pi^-\pi^+\eta)$		$1.25 \pm 0.08 \pm 0.07$	$1.26 \pm 0.11 \pm 0.08$	$1.33 \pm 0.39 \pm 0.20$
Data events	3722 ± 222	1605 ± 94	731 ± 62	197 ± 59
χ^2/NDF	77/62	50/43	61/55	39/43
Selection efficiency	$(8.3 \pm 0.1)\%$	$(3.75 \pm 0.04)\%$	$(2.97 \pm 0.05)\%$	$(0.53 \pm 0.06)\%$
Systematic uncertainties (%)				
Tracking efficiency	3.8	2.7	3.8	2.7
π^0 and η PID	...	3.0	3.0	9.0
Pion PID	2.5	1.5	2.5	1.5
Lepton-tag PID	1.6	1.6	1.6	1.6
N	1.0	1.0	1.0	1.0
Selection efficiency	0.6	1.1	1.6	11
Fit model	5.0	2.7	...	...
$\mathcal{B}(\eta \to \gamma\gamma)$	...	0.7	...	...
$\mathcal{B}(\eta \to \pi^+\pi^-\pi^0)$	...	...	1.2	...
$\mathcal{B}(\eta \to 3\pi^0)$	...	...	...	0.9
Total (%)	7.0	5.6	6.1	15

TABLE III. Results of fits for the mass of the f_1 resonance in $\tau^- \to \pi^- f_1 \nu_\tau$ decays. The errors are statistical.

Decay mode	Monte Carlo (generator-fit) (GeV/c^2)	Data (fit) (GeV/c^2)	Data (corrected) (GeV/c^2)
$f_1 \to 2\pi^+ 2\pi^-$	0.00074 ± 0.00008	1.28031 ± 0.00067	1.28105 ± 0.00067
$f_1 \to \pi^+\pi^-\eta$			
$\eta \to \gamma\gamma$	0.00292 ± 0.00040	1.27775 ± 0.00045	1.28067 ± 0.00060
$\eta \to \pi^+\pi^-\pi^0$	0.00018 ± 0.00020	1.27787 ± 0.00080	1.27805 ± 0.00082
$\eta \to 3\pi^0$	0.00347 ± 0.00033	1.28036 ± 0.00335	1.28383 ± 0.00337

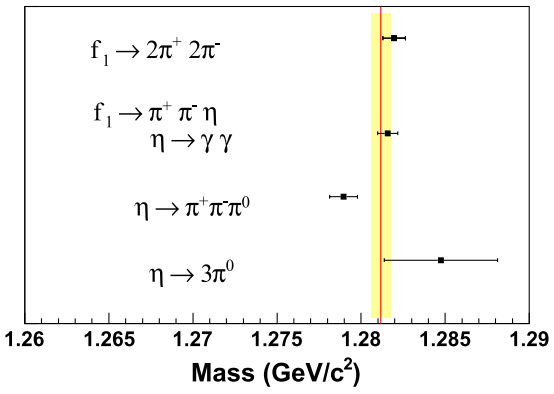

FIG. 3 (color online). Compilation of our measurements of the f_1 mass. The solid line is the weighted average and the shaded area is the one standard deviation region.

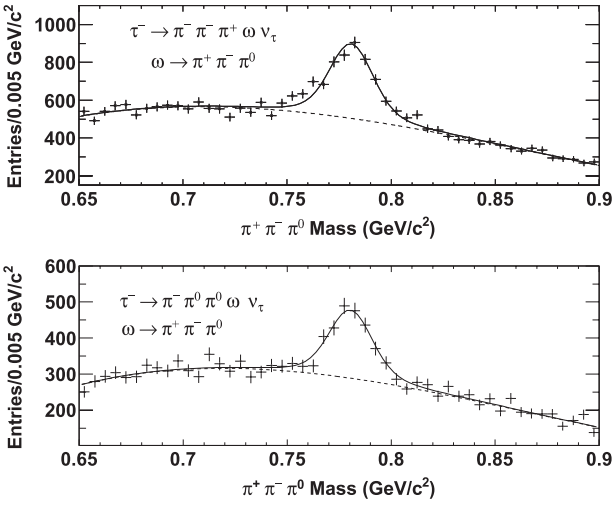

FIG. 4. The fits to the ω peak in the $\pi^+\pi^-\pi^0$ invariant mass distributions for $\tau^- \to 2\pi^-\pi^+\omega\nu_\tau$ and $\tau^- \to \pi^- 2\pi^0\omega\nu_\tau$ decay candidates after all selection criteria are applied. The solid lines represent the fit to the ω peak and background. The dashed lines show the extrapolation of the background function under the ω peak.

TABLE IV. Results and branching fractions for $\tau^- \to (3\pi)^- \omega \nu_\tau$ decays.

Decay mode	$\tau^- \to 2\pi^-\pi^+\omega\nu_\tau$ $\omega \to \pi^-\pi^+\pi^0$	$\tau^- \to \pi^- 2\pi^0\omega\nu_\tau$ $\omega \to \pi^-\pi^+\pi^0$
Branching fractions (10^{-5})	$8.4 \pm 0.4 \pm 0.6$	$7.3 \pm 1.2 \pm 1.2$
Data events	2372 ± 94	1135 ± 70
χ^2/NDF	55/44	42/44
Selection efficiency	$(3.27 \pm 0.03)\%$	$(0.75 \pm 0.01)\%$
Background	257 ± 71	709 ± 59
Systematic uncertainties (%)		
Tracking efficiency	3.8	2.7
π^0 and η PID	3.0	9.0
Pion PID	2.5	1.5
Lepton-tag PID	1.6	1.6
N	1.0	1.0
Selection efficiency	0.8	1.8
Background	3.4	14
$\mathcal{B}(\omega \to \pi^-\pi^+\pi^0)$	0.8	0.8
Total (%)	6.8	17

factor by fitting the η, ω, η', D^0 and D^{*-} states using data samples that have one track in the tag hemisphere and either three or five tracks in the signal hemisphere. No other selection criteria are applied. The peak masses are found to be lower than the known values by (-0.91 ± 0.10) MeV/c^2 and the values are independent of the mass of the resonance. We use the (-0.91 ± 0.10) MeV/c^2 as a correction factor that is applied to the invariant mass and its error is included in the systematic uncertainty.

We determine the mass of the $f_1(1258)$ meson to be

$$M_{f_1} = (1.28116 \pm 0.00039 \pm 0.00045)\ \text{GeV}/c^2.$$

The systematic uncertainty includes the reconstruction uncertainty and the calibration uncertainty. This result is in good agreement with the Particle Data Group value (1.2818 ± 0.0006) GeV/c^2 [11].

C. $\tau^- \to (3\pi)^- \omega \nu_\tau$

We measure the $\tau^- \to 2\pi^-\pi^+\omega\nu_\tau$ and $\tau^- \to \pi^- 2\pi^0\omega\nu_\tau$ branching fractions. The number of events is determined by fitting the ω peak in the $\pi^+\pi^-\pi^0$ invariant mass distributions (see Fig. 4) with a Breit-Wigner distribution, which is convolved with a Gaussian distribution to take into account the detector resolution. The resolution parameter of the Gaussian distribution is determined using a data control sample consisting of $q\bar{q}$ events, and is fixed in the fit. A polynomial function is used to fit the background. The results are presented in Table IV.

Approximately 10% of the events in the $\tau^- \to 2\pi^-\pi^+\omega\nu_\tau$ channel are backgrounds from other τ decays (primarily $\tau^- \to \pi^-\pi^0\omega\nu_\tau$ decays) and $e^+e^- \to q\bar{q}$ events. The backgrounds are subtracted before calculating the branching fraction.

The $\tau^- \to \pi^- 2\pi^0\omega\nu_\tau$ sample has substantial contributions from $\tau^- \to \pi^-\omega\nu_\tau$ and $\tau^- \to \pi^-\pi^0\omega\nu_\tau$ decays. The background is estimated with the Monte Carlo simulation and verified using data and simulation control samples. The control samples follow the nominal selection criteria but select one or two π^0 instead of three π^0 mesons.

The branching fractions are found to be

$$\mathcal{B}(\tau^- \to 2\pi^-\pi^+\omega\nu_\tau) = (8.4 \pm 0.4 \pm 0.6) \times 10^{-5},$$
$$\mathcal{B}(\tau^- \to \pi^- 2\pi^0\omega\nu_\tau) = (7.3 \pm 1.2 \pm 1.2) \times 10^{-5}.$$

The systematic uncertainties are listed in Table IV.

The $\tau^- \to 2\pi^-\pi^+\omega\nu_\tau$ and $\tau^- \to \pi^- 2\pi^0\omega\nu_\tau$ branching fractions are consistent with the results from CLEO, $(1.2 \pm 0.2 \pm 0.1) \times 10^{-4}$ and $(1.4 \pm 0.4 \pm 0.3) \times 10^{-4}$, respectively [14]. Gao and Li suggest that this mode is dominated by the $(\pi\rho\omega)$ state and predict a branching fraction in the range of $1.8 - 2.1 \times 10^{-4}$ with the two modes ($\tau^- \to 2\pi^-\pi^+\omega\nu_\tau$ and $\tau^- \to \pi^- 2\pi^0\omega\nu_\tau$) having the same value [23]. The result measured in this work is approximately 50% of the predicted rate but the ratio of the two branching fractions is consistent with unity.

D. Nonresonant decay modes

The resonant modes, involving η, ω and f_1 mesons, do not account for all of the observed decays, as discussed below. We consider the excess in the observed decays to be from ''nonresonant'' modes. We make no attempt to identify the contribution of resonances with larger widths (>100 MeV/c^2) as the nature of these resonances is complex and their line shapes will be modified by the limited phase space in the τ decay. The Monte Carlo simulation describes the final states using a phase-space model for the final-state particles. The only exception is the

TABLE V. Results and branching fractions for $\tau^- \to 2\pi^-\pi^+3\pi^0\nu_\tau$, $\tau^- \to 3\pi^-2\pi^+\nu_\tau$, and $\tau^- \to 3\pi^-2\pi^+\pi^0\nu_\tau$ nonresonant decays.

Decay mode	$\tau^- \to 2\pi^-\pi^+3\pi^0\nu_\tau$	$\tau^- \to 3\pi^-2\pi^+\nu_\tau$	$\tau^- \to 3\pi^-2\pi^+\pi^0\nu_\tau$
Branching fractions (10^{-4})	$0.10 \pm 0.08 \pm 0.30$	$7.68 \pm 0.04 \pm 0.40$	$0.36 \pm 0.03 \pm 0.09$
Data events	4094 ± 64	68985 ± 263	7296 ± 85
Efficiency	$(0.88 \pm 0.01)\%$	$(7.98 \pm 0.02)\%$	$(3.71 \pm 0.03)\%$
Background			
Resonant	1763 ± 222	4441 ± 370	4458 ± 244
Other τ decays	1681 ± 44	10621 ± 719	1315 ± 100
$q\bar{q}$	573 ± 50	1171 ± 205	359 ± 37
Total background	4017 ± 232	16233 ± 835	6132 ± 267
Systematic uncertainties (%)			
Tracking efficiency		3.8	3.8
π^0 and η PID		...	3.0
Pion PID		2.5	2.5
Lepton-tag PID		1.6	1.6
$\mathcal{L}\sigma_{\tau^+\tau^-}$		1.0	1.0
Selection efficiency		0.2	0.9
Background		1.6	22.9
Total (%)		5.2	23.7

$\tau^- \to 3\pi^-2\pi^+\nu_\tau$ mode, which Tauola models using $\tau^- \to a_1^-\nu_\tau$ decays [24].

We measure the branching fractions of the nonresonant $\tau^- \to 2\pi^-\pi^+3\pi^0\nu_\tau$, $\tau^- \to 3\pi^-2\pi^+\nu_\tau$, and $\tau^- \to 3\pi^-2\pi^+\pi^0\nu_\tau$ decays. The numbers of candidates are given by the numbers of events found in the data after subtracting the resonant contributions and the background from other τ decays and $q\bar{q}$ events (see Table V).

The invariant mass plots in Fig. 5 show that the resonant decays dominate the $\tau^- \to 2\pi^-\pi^+3\pi^0\nu_\tau$ mode. The background is primarily from $\tau^- \to \pi^-\pi^0\omega\nu_\tau$ and $q\bar{q}$ events. The branching fraction of the nonresonant $\tau^- \to 2\pi^-\pi^+3\pi^0\nu_\tau$ channel is determined to be $(1.0 \pm 0.8 \pm 3.0) \times 10^{-5}$. The systematic uncertainty on the branching fraction is dominated by the uncertainty in the background, which includes the Monte Carlo statistical uncertainty and the τ branching fraction uncertainties. We do not list the fractional systematic uncertainties for this mode in Table V due to the smallness of the branching fraction. The branching fraction is consistent with zero and we set a limit of

$$\mathcal{B}(\tau^- \to 2\pi^-\pi^+3\pi^0\nu_\tau) < 5.8 \times 10^{-5}$$

at the 90% confidence level.

We also determine the inclusive $\tau^- \to 2\pi^-\pi^+3\pi^0\nu_\tau$ branching fraction by summing the contribution from the three resonant modes $(B(\tau^- \to 2\pi^-\pi^+\eta\nu_\tau) \times B(\eta \to 3\pi^0) + B(\tau^- \to \pi^-2\pi^0\eta\nu_\tau)B(\eta \to \pi^+\pi^-\pi^0) + B(\tau^- \to \pi^-2\pi^0\omega\nu_\tau)B(\omega \to \pi^-\pi^+\pi^0))$ with the nonresonant branching fraction. We find the result $(2.07 \pm 0.18 \pm 0.37) \times 10^{-4}$, where the systematic uncertainty accounts for correlations between the systematic uncertainties of the individual modes.

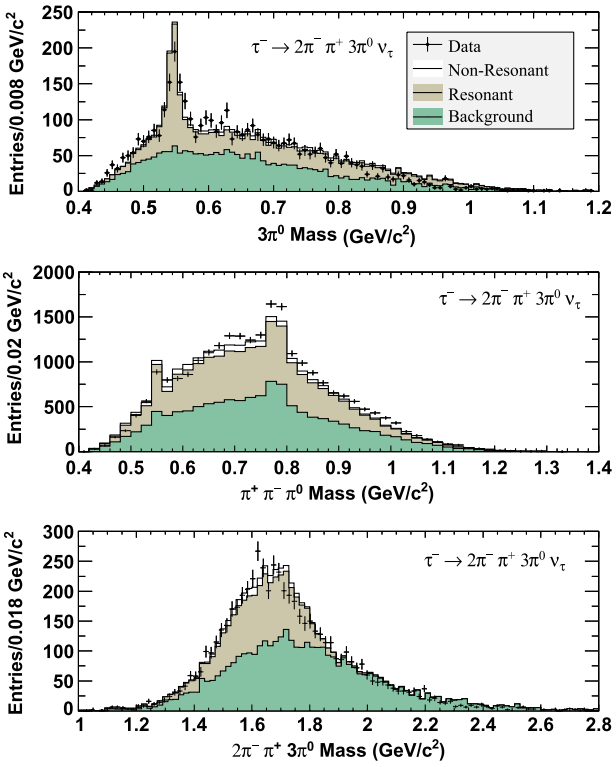

FIG. 5 (color online). The $3\pi^0$, $\pi^+\pi^-\pi^0$, and $2\pi^-\pi^+3\pi^0$ invariant mass distributions in $\tau^- \to 2\pi^-\pi^+3\pi^0\nu_\tau$ decay candidates. The predictions of the Monte Carlo simulation are shown for the resonant (white histogram) and nonresonant (light shaded histogram) τ decays, and the background from other τ decays and $q\bar{q}$ events (dark shaded histogram). The resonant decays include decays with the correct topology and a resonance (η, f_1 or ω) in the final state.

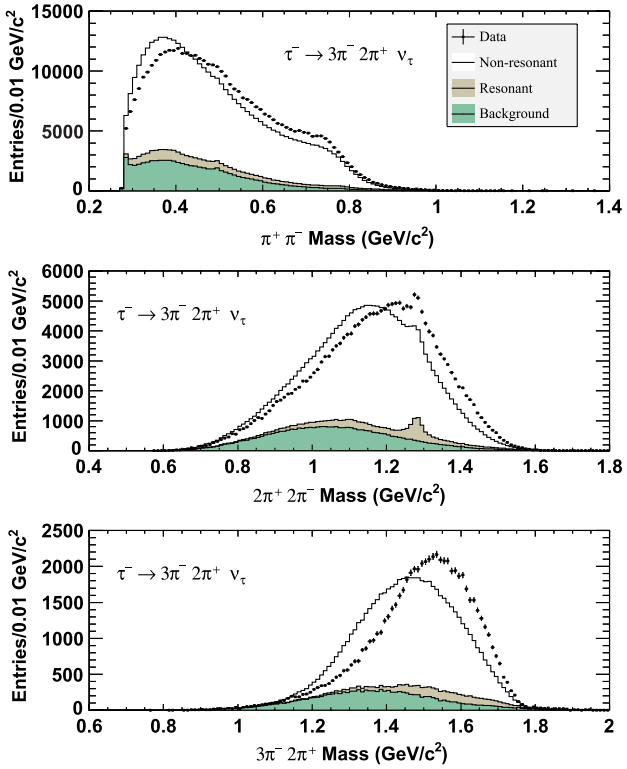

FIG. 6 (color online). The $\pi^+\pi^-$, $2\pi^+2\pi^-$, and $3\pi^-2\pi^+$ invariant mass distributions in $\tau^- \to 3\pi^-2\pi^+\nu_\tau$ decays. The predictions of the Monte Carlo simulation are shown for the resonant (white histogram) and nonresonant (light shaded histogram) τ decays, and the background from other τ decays and $q\bar{q}$ events (dark shaded histogram). The resonant decays include decays with the correct topology and a resonance (η, f_1 or ω) in the final state. The nonresonant decays are generated using $\tau^- \to a_1^-\nu_\tau$ events. The differences between the data and Monte Carlo predictions are discussed in the text.

The $\tau^- \to 3\pi^-2\pi^+\nu_\tau$ decay has only a small contribution from resonant decays (see Fig. 6). The branching fraction of the nonresonant $\tau^- \to 3\pi^-2\pi^+\nu_\tau$ decay is determined to be

$$\mathcal{B}(\tau^- \to 3\pi^-2\pi^+\nu_\tau) = (7.68 \pm 0.04 \pm 0.40) \times 10^{-4}.$$

Although the modeling of the $3\pi^-2\pi^+$ invariant mass distribution is deficient, the selection efficiency remains the same if the Monte Carlo is reweighted to resemble the data distribution. The decay model represents a significant improvement compared to a phase-space model, in which the ρ meson, observed in the $\pi^+\pi^-$ invariant mass spectrum, is not included. Further tuning of the model is required, which is outside the scope of the present study. The background from the $q\bar{q}$ events is validated by comparing the numbers of data and Monte Carlo events in the region above the τ lepton mass.

The inclusive $\tau^- \to 3\pi^-2\pi^+\nu_\tau$ branching fraction is $(8.33 \pm 0.04 \pm 0.43) \times 10^{-4}$ and is obtained using the same method as the nonresonant branching fraction except that the $\tau^- \to \pi^- f_1\nu_\tau$ decays (the only resonant decay in this channel) is considered as a background. In addition, the contribution of the $\tau^- \to 2\pi^-\pi^+\omega\nu_\tau$ decay via the $\omega \to \pi^+\pi^-$ mode is negligible. The branching fraction of the $\tau^- \to 3h^-2h^+\nu_\tau$ decay (where h^- is either a π^- or K^-) was measured to be $(8.56 \pm 0.05 \pm 0.42) \times 10^{-4}$ in a previous *BABAR* analysis [18] using a smaller data sample, which did not use charged particle identification.

$\tau^- \to 3\pi^-2\pi^+\pi^0\nu_\tau$ decays are dominated by the resonant modes (see Fig. 7). We determine the branching fraction of the nonresonant $\tau^- \to 3\pi^-2\pi^+\pi^0\nu_\tau$ decay mode to be

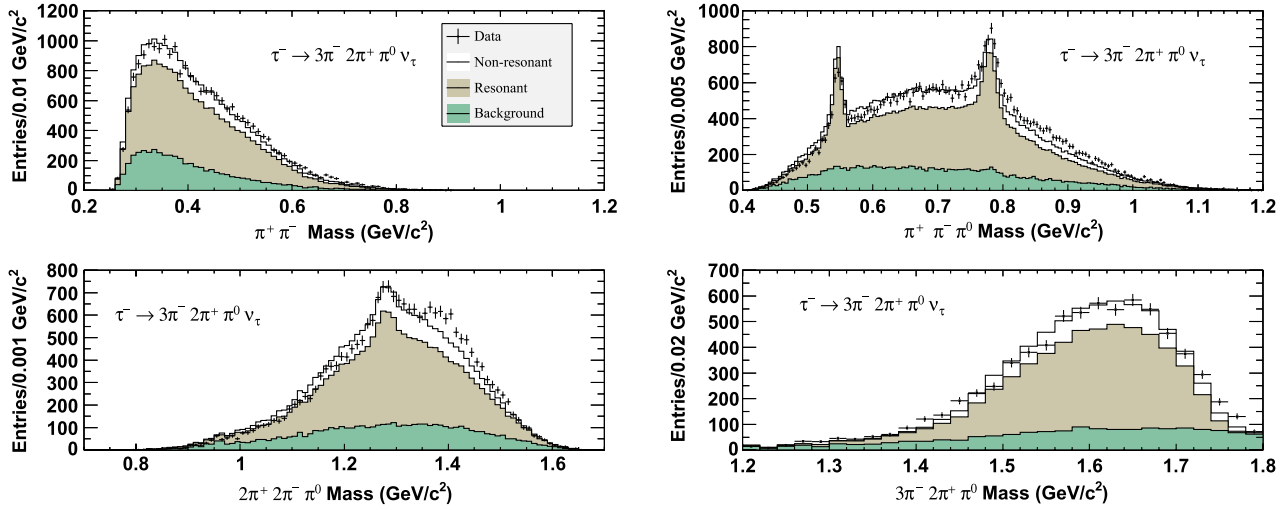

FIG. 7 (color online). The $\pi^+\pi^-$, $\pi^+\pi^-\pi^0$, $2\pi^-2\pi^+\pi^0$, and $3\pi^-2\pi^+\pi^0$ invariant mass distributions in $\tau^- \to 3\pi^-2\pi^+\pi^0\nu_\tau$ decays. The predictions of the Monte Carlo simulation are shown for the resonant (white histogram) and nonresonant (light shaded histogram) τ decays, and the background from other τ decays and $q\bar{q}$ events (dark shaded histogram). The resonant decays include decays with correct topology and a resonance (η, f_1 or ω) in the final state.

TABLE VI. Results and branching fractions for $\tau^- \to \pi^-\pi^0\eta'(958)\nu_\tau$, $\tau^- \to K^-\eta'(958)\nu_\tau$, and $\tau^- \to \pi^-\eta'(958)\nu_\tau$ decays.

$\tau^- \to \pi^-\pi^0\eta'(958)\nu_\tau$	$\eta \to \gamma\gamma$	$\eta \to \pi^+\pi^-\pi^0$	
Limit (90% C.L.)	$<1.4 \times 10^{-5}$	$<1.9 \times 10^{-5}$	
Branching fraction (10^{-6})	$7.8 \pm 4.1 \pm 1.7$	$0.0 \pm 7.6 \pm 9.3$	
Data events	24 ± 10	5 ± 6	
Background events	5 ± 7	5 ± 8	
Selection efficiency	$(1.58 \pm 0.02)\%$	$(1.00 \pm 0.03)\%$	
$\tau^- \to K^-\eta'(958)\nu_\tau$	$\eta \to \gamma\gamma$	$\eta \to \pi^+\pi^-\pi^0$	
Limit (90% C.L.)	$<2.4 \times 10^{-6}$	$<4.2 \times 10^{-6}$	
Branching fraction (10^{-6})	$0.5 \pm 1.3 \pm 0.4$	$1.6 \pm 1.4 \pm 1.2$	
Data events	6 ± 7	15 ± 4	
Background events	3 ± 4	11 ± 3	
Selection efficiency	$(3.47 \pm 0.03)\%$	$(3.09 \pm 0.04)\%$	
$\tau^- \to \pi^-\eta'(958)\nu_\tau$	$\eta \to \gamma\gamma$	$\eta \to \pi^+\pi^-\pi^0$	$\eta \to 3\pi^0$
Limit (90% C.L.)	$<5.2 \times 10^{-6}$	$<9.0 \times 10^{-6}$	$<1.3 \times 10^{-5}$
Branching fraction (10^{-6})	$-2.8 \pm 3.5 \pm 1.9$	$-0.4 \pm 3.9 \pm 4.3$	$-1.8 \pm 8.1 \pm 3.3$
Data events	40 ± 22	44 ± 11	12 ± 10
Background events	58 ± 12	45 ± 12	14 ± 4
Selection efficiency	$(4.06 \pm 0.35)\%$	$(3.25 \pm 0.15)\%$	$(0.96 \pm 0.10)\%$

$$\mathcal{B}(\tau^- \to 3\pi^- 2\pi^+\pi^0\nu_\tau) = (3.6 \pm 0.3 \pm 0.9) \times 10^{-5}.$$

The systematic uncertainty on the nonresonant $\tau^- \to 3\pi^- 2\pi^+\pi^0\nu_\tau$ branching fraction is dominated by the large uncertainty in the background (see Table V). Although the invariant mass distributions of the resonant modes in the Monte Carlo simulation are corrected to provide better agreement with the data, the corrections make little difference to the final branching fraction result. The other τ decays and the $q\bar{q}$ events contribute to a lesser extent; their contribution to the uncertainty of the background is very small.

The $\tau^- \to 3\pi^- 2\pi^+\pi^0\nu_\tau$ (including ω and excluding η) branching fraction is $(1.11 \pm 0.04 \pm 0.09) \times 10^{-4}$ and is obtained by adding the nonresonant branching fraction and the resonant branching fraction attributed to the $\tau^- \to 2\pi^-\pi^+\omega\nu_\tau$ via $\omega \to \pi^-\pi^+\pi^0$ decay.

The inclusive $\tau^- \to 3\pi^- 2\pi^+\pi^0\nu_\tau$ branching fraction is $(1.65 \pm 0.05 \pm 0.09) \times 10^{-4}$ and is obtained by adding the nonresonant branching fraction with the resonant branching fractions $(B(\tau^- \to 2\pi^-\pi^+\eta\nu_\tau)B(\eta \to \pi^+\pi^-\pi^0) + B(\tau^- \to 2\pi^-\pi^+\omega\nu_\tau)B(\omega \to \pi^-\pi^+\pi^0))$.

The $\tau^- \to 3\pi^- 2\pi^+\pi^0\nu_\tau$ (including ω and excluding η) branching fraction can be compared with isospin model predictions [25,26]. There are three τ decay modes with six pions in the final state: $\tau^- \to 2\pi^-\pi^+ 3\pi^0\nu_\tau$, $\tau^- \to 3\pi^- 2\pi^+\pi^0\nu_\tau$, and $\tau^- \to \pi^- 5\pi^0\nu_\tau$ (there are no measurements of the $\tau^- \to \pi^- 5\pi^0\nu_\tau$ decay mode). There are four possible isospin states for six pion decays: $(4\pi\rho)$, (3ρ), $(3\pi\omega)$, and $(\pi\rho\omega)$. The relative rates of the decays can be used to identify the dominant isospin states. The approximate equality of the $\tau^- \to 2\pi^-\pi^+ 3\pi^0\nu_\tau$ and $\tau^- \to 3\pi^- 2\pi^+\pi^0\nu_\tau$ branching fractions suggest that the $(4\pi\rho)$ and $(\pi\rho\omega)$ modes should dominate. The limited

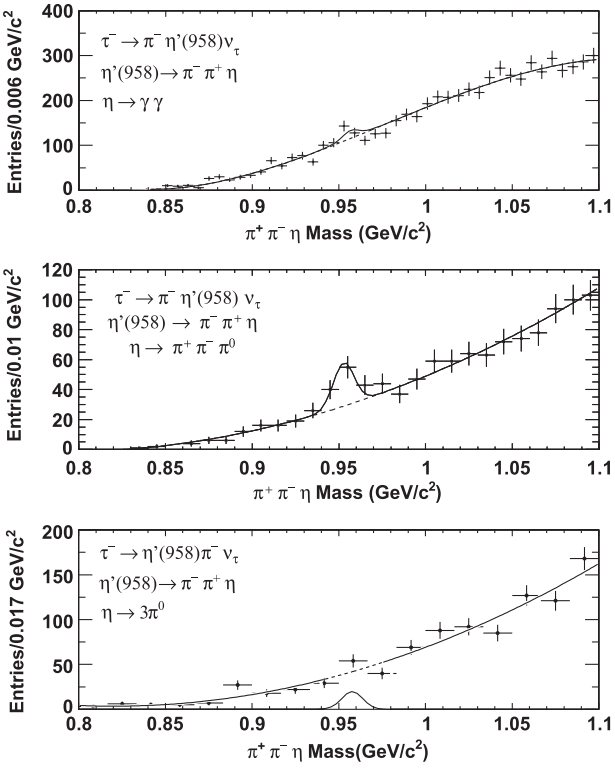

FIG. 8. The $\pi^+\pi^-\eta$ invariant mass in $\tau^- \to 2\pi^-\pi^+\eta\nu_\tau$ decay candidates for the $\eta \to \gamma\gamma$, $\eta \to \pi^+\pi^-\pi^0$, and $\eta \to 3\pi^0$ decay modes after all selection criteria are applied. The fit to the η' peak (in the top two plots) is represented by the solid line. The number of η' candidates in the $\eta \to 3\pi^0$ channel is determined by counting the number of events in a single bin centered on the η' mass and subtracting the combinatorial events. The number of combinatorial events is determined by fitting the data (the solid line in the bottom plot), excluding the data point near the η' peak. The peak in this plot indicates the expected location and width of an η' signal.

phase space imposed by the τ mass suppresses the higher mass states and as a result we do not observe evidence of the ρ meson in these decays.

E. Search for decays involving η' (958) decays

We also search for the $\tau^- \to \pi^-\pi^0\eta'(958)\nu_\tau$, $\tau^- \to K^-\eta'(958)\nu_\tau$, and $\tau^- \to \pi^-\eta'(958)\nu_\tau$ decays, where $\eta' \to \pi^-\pi^+\eta$. The first two decays are allowed first-class current decays whereas the last decay is a second-class current decay, with a rate that would be zero in the limit of perfect isospin symmetry.

The numbers of η' candidates in the data and background Monte Carlo samples are given in Table VI. For the $\tau^- \to \pi^-\pi^0\eta'(958)\nu_\tau$ via $\eta \to \gamma\gamma$ and the $\tau^- \to \pi^-\eta'(958)\nu_\tau$ via $\eta \to \gamma\gamma$ and $\eta \to \pi^+\pi^-\pi^0$ modes, we measure the number of η' candidates by fitting the peak with a Gaussian function and the combinatoric background with a polynomial function. The number of η' candidates in the other channels is determined by counting the number of events in a single bin centered on the η' mass and subtracting the combinatorial events. The level of the combinatorial background is estimated by fitting the mass spectrum or from the average level of the sideband region around the η' peak.

The $\pi^+\pi^-\eta$ invariant mass distributions for the $\tau^- \to \pi^-\eta'(958)\nu_\tau$ candidate decays are shown in Fig. 8. Although we see an η' peak in the $\eta \to \pi^+\pi^-\pi^0$ channel, we find that it can be fully accounted for by $q\bar{q}$ events. We do not show the invariant mass distributions for the $\tau^- \to \pi^-\pi^0\eta'(958)\nu_\tau$ and $\tau^- \to K^-\eta'(958)\nu_\tau$ decays. The analysis of these decay modes uses only the $\eta \to \gamma\gamma$ and $\eta \to \pi^+\pi^-\pi^0$ channels. The $\eta \to 3\pi^0$ channel was not considered due to the limited size of the samples.

The results for the three decay modes are given in Table VI. The selection efficiencies are determined with the signal Monte Carlo samples. The backgrounds from η' mesons are attributed to $e^+e^- \to q\bar{q}$ events and estimated using the Monte Carlo samples. The background estimations are validated by comparing the prediction of the Monte Carlo simulation with data for events where the invariant mass of all the observed final-state particles is greater than the τ mass.

We find no evidence for $\tau^- \to \pi^-\pi^0\eta'(958)\nu_\tau$, $\tau^- \to K^-\eta'(958)\nu_\tau$, or $\tau^- \to \pi^-\eta'(958)\nu_\tau$ decays (see Table VI) and place the following upper limits on the branching fractions at the 90% confidence level:

$$\mathcal{B}(\tau^- \to \pi^-\pi^0\eta'(958)\nu_\tau) < 1.2 \times 10^{-5},$$
$$\mathcal{B}(\tau^- \to K^-\eta'(958)\nu_\tau) < 2.4 \times 10^{-6},$$
$$\mathcal{B}(\tau^- \to \pi^-\eta'(958)\nu_\tau) < 4.0 \times 10^{-6}.$$

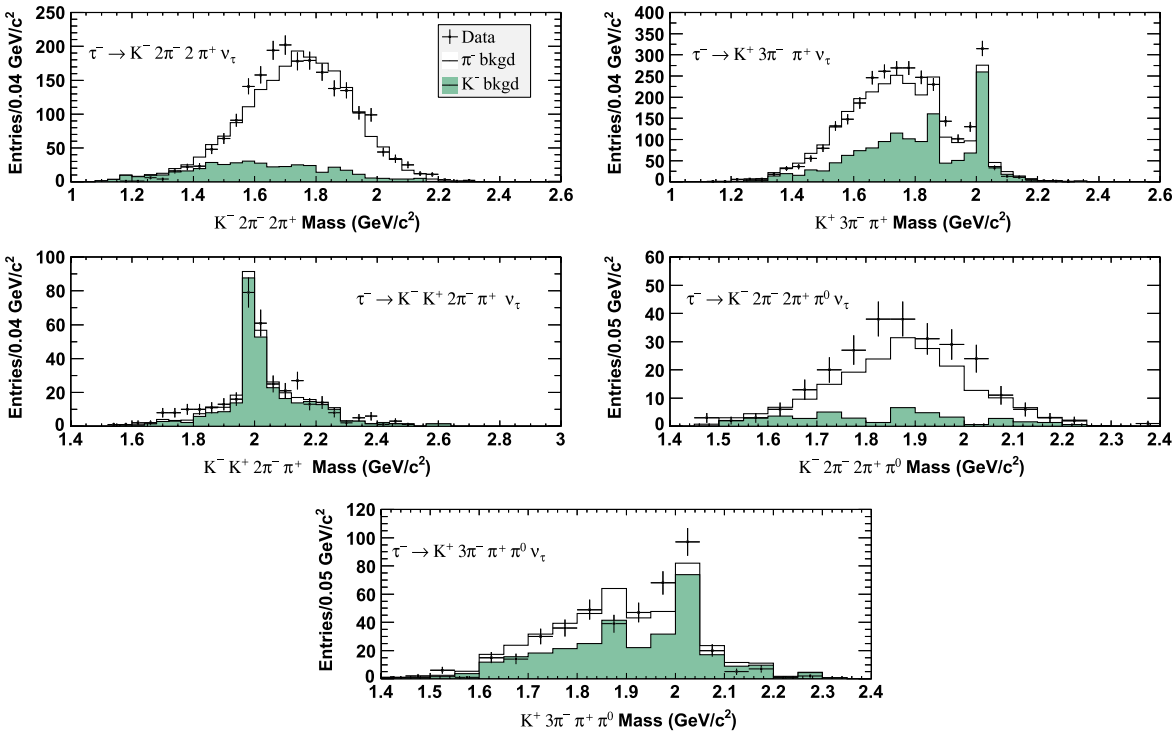

FIG. 9 (color online). The $K^-2\pi^-2\pi^+$, $K^+3\pi^-\pi^+$, $K^-K^+2\pi^-\pi^+$, $K^-2\pi^-2\pi^+\pi^0$, and $K^+3\pi^-\pi^+\pi^0$ invariant mass distributions in the data sample after all selection criteria are applied. The unshaded histogram represents τ decays in which a charged pion is misidentified as a charged kaon, and the shaded histograms are primarily from $q\bar{q}$ events in which there is a charged kaon in the final state. The Monte Carlo simulation does not include signal decays.

TABLE VII. Results and branching fractions for charged kaon decay modes.

Decay mode	$\tau^- \to K^- 2\pi^- 2\pi^+ \nu_\tau$	$\tau^- \to K^+ 3\pi^- \pi^+ \nu_\tau$	$\tau^- \to K^- K^+ 2\pi^- \pi^+ \nu_\tau$
Limit (90% C.L.)	$<2.4 \times 10^{-6}$	$<5.0 \times 10^{-6}$	$<4.5 \times 10^{-7}$
Branching fraction (10^{-6})	$0.6 \pm 0.5 \pm 1.1$	$1.6 \pm 0.6 \pm 2.4$	$0.30 \pm 0.10 \pm 0.07$
Data events	1328 ± 36	1999 ± 45	32 ± 6
Background	1284 ± 72	1890 ± 163	15 ± 4
Selection efficiency	$(7.9 \pm 0.1)\%$	$(7.9 \pm 0.1)\%$	$(6.7 \pm 0.1)\%$
	$\tau^- \to K^- 2\pi^- 2\pi^+ \pi^0 \nu_\tau$	$\tau^- \to K^+ 3\pi^- \pi^+ \pi^0 \nu_\tau$	
Limit (90% C.L.)	$<1.9 \times 10^{-6}$	$<8 \times 10^{-7}$	
Branching fraction (10^{-6})	$1.1 \pm 0.4 \pm 0.4$	$-0.6 \pm 0.5 \pm 0.7$	
Data events	112 ± 11	154 ± 12	
Background	84 ± 10	170 ± 16	
Selection efficiency	$(2.9 \pm 0.1)\%$	$(2.9 \pm 0.1)\%$	

The limits are determined from the weighted average of the branching fractions measured for each mode. The $\tau^- \to \pi^- \pi^0 \eta'(958) \nu_\tau$ and $\tau^- \to K^- \eta'(958) \nu_\tau$ channels are potential backgrounds to the $\tau^- \to \pi^- \eta'(958) \nu_\tau$ decay. We find that background from these two decays is less than two events based on the upper limits on the branching fractions and we consider these backgrounds to be negligible. The previous limits on the $\tau^- \to \pi^- \eta'(958) \nu_\tau$ decay were measured by *BABAR* to be $<7.2 \times 10^{-6}$ [13] and by CLEO to be $<8 \times 10^{-5}$ [19]. It is predicted that the branching fraction of $\tau^- \to \pi^- \eta'(958) \nu_\tau$ should be less than 1.4×10^{-6} [27].

TABLE VIII. Summary of branching fractions excluding contributions from $K^0_S \to \pi^+ \pi^-$.

Decay mode	Branching fraction
Resonant decays	
$\tau^- \to 2\pi^- \pi^+ \eta \nu_\tau$ (including f_1)	$(2.25 \pm 0.07 \pm 0.12) \times 10^{-4}$
$\tau^- \to 2\pi^- \pi^+ \eta \nu_\tau$ (excluding f_1)	$(0.99 \pm 0.09 \pm 0.13) \times 10^{-4}$
$\tau^- \to \pi^- 2\pi^0 \eta \nu_\tau$ (including f_1)	$(2.01 \pm 0.34 \pm 0.22) \times 10^{-4}$
$\tau^- \to \pi^- f_1 \nu_\tau$ via $f_1 \to 2\pi^+ 2\pi^-$	$(5.20 \pm 0.31 \pm 0.37) \times 10^{-5}$
$\tau^- \to \pi^- f_1 \nu_\tau$ via $f_1 \to \pi^+ \pi^- \eta$	$(1.26 \pm 0.06 \pm 0.06) \times 10^{-4}$
$\mathcal{B}(f_1 \to 2\pi^+ 2\pi^-)/\mathcal{B}(f_1 \to \pi\pi\eta)$	$0.28 \pm 0.02 \pm 0.02$
$\tau^- \to 2\pi^- \pi^+ \omega \nu_\tau$	$(8.4 \pm 0.4 \pm 0.6) \times 10^{-5}$
$\tau^- \to \pi^- 2\pi^0 \omega \nu_\tau$	$(7.3 \pm 1.2 \pm 1.2) \times 10^{-5}$
Nonresonant decays	
$\tau^- \to 3\pi^- 2\pi^+ \nu_\tau$ (excluding ω, f_1)	$(7.68 \pm 0.04 \pm 0.40) \times 10^{-4}$
$\tau^- \to 2\pi^- \pi^+ 3\pi^0 \nu_\tau$ (excluding η, ω, f_1)	$(1.0 \pm 0.8 \pm 3.0) \times 10^{-5}$
$\tau^- \to 2\pi^- \pi^+ 3\pi^0 \nu_\tau$ (excluding η, f_1)	$(16.9 \pm 0.8 \pm 4.3) \times 10^{-5}$
$\tau^- \to 3\pi^- 2\pi^+ \pi^0 \nu_\tau$ (excluding η, ω, f_1)	$(3.6 \pm 0.3 \pm 0.9) \times 10^{-5}$
$\tau^- \to 3\pi^- 2\pi^+ \pi^0 \nu_\tau$ (excluding η, f_1)	$(1.11 \pm 0.04 \pm 0.09) \times 10^{-4}$
Inclusive decays (including η, ω, f_1)	
$\tau^- \to 2\pi^- \pi^+ 3\pi^0 \nu_\tau$	$(2.07 \pm 0.18 \pm 0.37) \times 10^{-4}$
$\tau^- \to 3\pi^- 2\pi^+ \nu_\tau$ (excluding ω)	$(8.33 \pm 0.04 \pm 0.43) \times 10^{-4}$
$\tau^- \to 3\pi^- 2\pi^+ \pi^0 \nu_\tau$	$(1.65 \pm 0.05 \pm 0.09) \times 10^{-4}$
η' (958) decays (90% upper level confidence limit)	
$\tau^- \to \pi^- \pi^0 \eta'(958) \nu_\tau$	$<1.2 \times 10^{-5}$
$\tau^- \to K^- \eta'(958) \nu_\tau$	$<2.4 \times 10^{-6}$
$\tau^- \to \pi^- \eta'(958) \nu_\tau$	$<4.0 \times 10^{-6}$
Kaonic decays (90% upper level confidence limit)	
$\tau^- \to K^- 2\pi^- 2\pi^+ \nu_\tau$	$<2.4 \times 10^{-6}$
$\tau^- \to K^+ 3\pi^- \pi^+ \nu_\tau$	$<5.0 \times 10^{-6}$
$\tau^- \to K^- K^+ 2\pi^- \pi^+ \nu_\tau$	$<4.5 \times 10^{-7}$
$\tau^- \to K^- 2\pi^- 2\pi^+ \pi^0 \nu_\tau$	$<1.9 \times 10^{-6}$
$\tau^- \to K^+ 3\pi^- \pi^+ \pi^0 \nu_\tau$	$<8 \times 10^{-7}$

F. Searches for decays involving charged kaons

Finally we present the first search for high-multiplicity τ decays with one or two charged kaons. We find no evidence for signal decays and place upper limits on the branching fractions of the $\tau^- \to K^- 2\pi^- 2\pi^+ \nu_\tau$, $\tau^- \to K^+ 3\pi^- \pi^+ \nu_\tau$, $\tau^- \to K^- K^+ 2\pi^- \pi^+ \nu_\tau$, $\tau^- \to K^- 2\pi^- 2\pi^+ \pi^0 \nu_\tau$, $\tau^- \to K^+ 3\pi^- \pi^+ \pi^0 \nu_\tau$, and $\tau^- \to K^- \eta'(958) \nu_\tau$ decay modes (the $\tau^- \to K^- \eta'(958) \nu_\tau$ decay was presented in Sec. III E).

The events are divided into topologies in which the charged kaon has either the same or opposite charge as the parent τ lepton. If there are two kaon candidates, they must have opposite charge. All other tracks are required to be identified as charged pions. The selection criteria and systematic uncertainties are described earlier. The requirement on the invariant mass ($M < 1.8$ GeV$/c^2$) of the final state uses the kaon mass for tracks identified as charged kaons. Figure 9 shows the mass spectra for the various channels. The predictions of the Monte Carlo simulation are divided into decays with or without a K^- (in this latter case, a π^- is misidentified as a K^-). The figures do not include any signal decays in the Monte Carlo samples. The background estimates, which give the dominant systematic uncertainty, are verified by comparing the numbers of events in the data and Monte Carlo samples in the $M > 1.8$ GeV$/c^2$ region.

The numbers of events selected in the data and Monte Carlo simulations are given in Table VII. The backgrounds predicted by the Monte Carlo simulations are approximately equal to the numbers of events in the data sample. There is an excess of data events in the $\tau^- \to K^- 2\pi^- 2\pi^+ \pi^0 \nu_\tau$ mode, but this excess extends to mass values above the τ mass, indicating that events are due to background τ decays or $q\bar{q}$ events.

The upper limits on the branching fractions are given in Table VII. There are no predictions for these modes. We estimate that $\mathcal{B}(\tau^- \to K^- 2\pi^- 2\pi^+ \nu_\tau) \sim 10^{-5}$–$10^{-6}$ if the decay is related to $\mathcal{B}(\tau^- \to 3\pi^- 2\pi^+ \nu_\tau)$ by the ratio of the Cabibbo-Kobayashi-Maskawa matrix elements (V_{us}/V_{ud}). The $\tau^- \to 3\pi^- 2\pi^+ \pi^0 \nu_\tau$ decay is dominated by decays to the narrow low-lying resonances and the branching fraction of decay modes created by replacing a π^- with K^- would be highly suppressed due to the limited phase space.

IV. SUMMARY

We present measurements of the branching fractions for τ lepton decays to three-prong and five-prong final states. The results are summarized in Table VIII. The branching fractions exclude contributions of the K^0_S meson. The results are more precise than previous measurements and many decay modes are studied for the first time.

ACKNOWLEDGMENTS

We are grateful for the extraordinary contributions of our PEP-II colleagues in achieving the excellent luminosity and machine conditions that have made this work possible. The success of this project also relies critically on the expertise and dedication of the computing organizations that support *BABAR*. The collaborating institutions wish to thank SLAC for its support and the kind hospitality extended to them. This work is supported by the U.S. Department of Energy and National Science Foundation, the Natural Sciences and Engineering Research Council (Canada), the Commissariat à l'Energie Atomique and Institut National de Physique Nucléaire et de Physique des Particules (France), the Bundesministerium für Bildung und Forschung and Deutsche Forschungsgemeinschaft (Germany), the Istituto Nazionale di Fisica Nucleare (Italy), the Foundation for Fundamental Research on Matter (The Netherlands), the Research Council of Norway, the Ministry of Education and Science of the Russian Federation, Ministerio de Ciencia e Innovación (Spain), and the Science and Technology Facilities Council (United Kingdom). Individuals have received support from the Marie-Curie IEF program (European Union) and the A. P. Sloan Foundation (USA).

[1] S. Banerjee, B. Pietrzyk, J. M. Roney, and Z. Wąs, Phys. Rev. D **77**, 054012 (2008).
[2] B. Aubert *et al.* (*BABAR* Collaboration), Nucl. Instrum. Methods Phys. Res., Sect. A **479**, 1 (2002).
[3] B. Aubert *et al.* (*BABAR* Collaboration), Phys. Rev. Lett. **99**, 021603 (2007).
[4] S. Jadach, B. F. L. Ward, and Z. Wąs, Comput. Phys. Commun. **130**, 260 (2000).
[5] S. Jadach, Z. Wąs, R. Decker, and J. H. Kühn, Comput. Phys. Commun. **76**, 361 (1993).
[6] T. Sjöstrand, Comput. Phys. Commun. **82**, 74 (1994).
[7] E. Barberio and Z. Wąs, Comput. Phys. Commun. **79**, 291 (1994).
[8] D. J. Lange, Nucl. Instrum. Methods Phys. Res., Sect. A **462**, 152 (2001).
[9] S. Agostinelli *et al.* (GEANT4 Collaboration), Nucl. Instrum. Methods Phys. Res., Sect. A **506**, 250 (2003).
[10] S. Brandt, Ch. Peyrou, R. Sosnowski, and A. Wroblewski, Phys. Lett. **12**, 57 (1964); E. Farhi, Phys. Rev. Lett. **39**, 1587 (1977).
[11] J. Beringer *et al.* (Particle Data Group), Phys. Rev. D **86**, 010001 (2012).

[12] The Novosibirsk function is defined as $f(m) = A\exp(-0.5\{\ln^2[1+\Lambda\tau\cdot(m-m_0)]/\tau^2+\tau^2\})$, where $\Lambda = \sinh(\tau\sqrt{\ln 4})/(\sigma\tau\sqrt{\ln 4})$, the peak position is m_0, the width is σ and τ is the tail parameter.
[13] B. Aubert *et al.* (*BABAR* Collaboration), Phys. Rev. D **77**, 112002 (2008).
[14] A. Anastassov *et al.* (CLEO Collaboration), Phys. Rev. Lett. **86**, 4467 (2001).
[15] B. A. Li, Phys. Rev. D **57**, 1790 (1998).
[16] M. Acciarri *et al.* (L3 Collaboration), Phys. Lett. B **501**, 1 (2001).
[17] $\mathcal{B}(f_1 \to \pi^+\pi^-\eta) = 0.349^{+0.013}_{-0.015}$ is obtained by taking two-thirds of $\mathcal{B}(f_1 \to \pi\pi\eta) = 0.524^{+0.019}_{-0.021}$ from Ref. [11].
[18] B. Aubert *et al.* (*BABAR* Collaboration), Phys. Rev. D **72**, 072001 (2005).
[19] T. Bergfeld *et al.* (CLEO Collaboration), Phys. Rev. Lett. **79**, 2406 (1997).
[20] B. A. Li, Phys. Rev. D **55**, 1436 (1997).
[21] B. Aubert *et al.* (*BABAR* Collaboration), Phys. Rev. D **76**, 092005 (2007).
[22] B. Aubert *et al.* (*BABAR* Collaboration), Phys. Rev. D **80**, 092005 (2009).
[23] J. Gao and B. A. Li, Eur. Phys. J. C **22**, 283 (2001).
[24] J. H. Kühn and Z. Wąs, Acta Phys. Pol. B **39**, 147 (2008).
[25] A. Pais, Ann. Phys. (N.Y.) **9**, 548 (1960).
[26] R. J. Sobie, Phys. Rev. D **60**, 017301 (1999).
[27] S. Nussinov and A. Soffer, Phys. Rev. D **80**, 033010 (2009).